Directed Assembly of P3HT:PCBM Blend Films Using A Chemical Template with Sub-300 nm Features

David S. Germack,[†,‡,*] Antonio Checco,[‡,*] and Benjamin M. Ocko

Condensed Matter Physics and Materials Science Department, Brookhaven National Laboratory, Upton, New York 11973, United States. [‡]These authors contributed equally. Present address: [†]CESI Chemical, The Woodlands, TX 77381, United States.

ABSTRACT Surface energy has been demonstrated as a means to direct interfacial-layer composition in polymer:fullerene blends utilized as active layers in organic photovoltaic devices. Combined with recent materials advances in the preparation of nanoscale chemical patterns, surface energy control of nanophase separation presents an opportunity to employ patterned surface energy templates to control the 3D blend morphology of polymer:fullerene blends. This report details the directed assembly of poly(3-hexylthiophene):phenyl-C_{61}-butyric acid methyl ester (P3HT:PCBM) blends atop linear grating patterns with domains of alternating high and low surface energy of 50 to 600 nm in width prepared by nanoscale oxidative lithography of alkyl-terminated self-assembled monolayers on SiO_2 and SiH surfaces. Tapping-, contact-, and current-sensing AFM studies demonstrated that chemical patterns were effective at directing the 3D morphology of P3HT:PCBM blends at dimensions of >200 nm. As the dimensionality of domains approached 100 nm, the chemical patterns were no longer able to direct phase segregation, evidence that a directed spinodal decomposition mechanism was responsible for the observed morphology. Surprisingly, the low surface energy component (P3HT) was found to be atop the high surface energy domains of the template, in conflict with current understanding of the role of surface energy directed assembly in polymer blends. These results suggest that the directed spinodal decomposition mechanism applies to conjugated polymer:fullerene blends, but that additional parameters unique to these types of systems will require refinement of the theory to adequately describe and predict the behavior of these scientifically and industrially interesting materials.

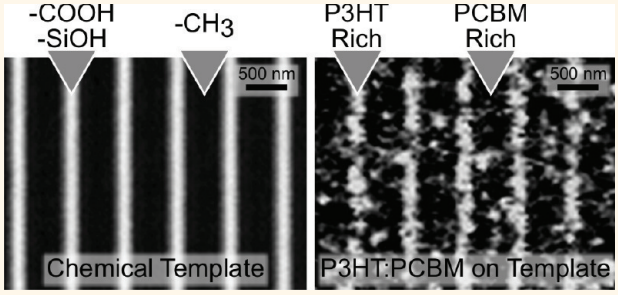

KEYWORDS: templated self-assembly · current-sensing AFM · nanolithography · bulk heterojunction · nanocomposites

Control over the nanoscale morphology of soft (*i.e.*, organic, polymeric, and biological) thin-film materials is crucial for achieving desired functionality or performance. For nanocomposites intended for application in organic photovoltaic (OPV) devices, morphological control (*i.e.*, control of the dimensionality, distribution, orientation, and continuity of domains) is critical, as the nanoscale morphology of the bulk-heterojunction active layer is directly related to the effectiveness of charge carrier separation and collection, and thus the efficiency of the device.[1]

The morphology of conjugated polymer blends with phenyl-C_{61}–butyric acid methyl ester (PCBM) is typically controlled by kinetically arrested nanoscale phase separation before thermodynamic equilibrium is reached. The use of arrested nanoscale phase separation has several drawbacks, including that a thermodynamically unstable morphology might coarsen over time to a morphology that has diminished functionality. It is difficult to construct phase diagrams of polymer:PCBM blends or to construct reasonable models to simulate phase segregation because Flory–Huggins theory alone cannot describe the phase behavior of semicrystalline rigid-rod polymer blends with hard spheres.[2,3] Complicating this scenario are the narrow collection of good solvents for PCBM and most semiconducting polymers, the wide molecular weight distributions of most semiconducting polymers, and the semicrystalline nature of PCBM and semiconducting polymers. Reliance on the phase-separation route to set the morphology of polymer:PCBM blends has therefore resulted in unpredictable results, with a large distribution of domain

* Address correspondence to dsgermack@gmail.com; checco@bnl.gov.

Received for review August 17, 2012 and accepted January 7, 2013.

Published online January 08, 2013
10.1021/nn303765t

dimensionality, orientation, distribution, and composition, even in widely studied systems such as poly(3-hexylthiophene) (P3HT) blends with PCBM.[4−6] This is reflected in the empirical optimization strategies that must be applied to each new polymer:PCBM blend in order to determine processing conditions that result in high-efficiency devices. On the other hand, optimized recipes for polymer:PCBM blends often result in complex phase behavior that further complicates development of structure−property relationships of morphology and performance. For example, P3HT:PCBM blends with optimal performance are a three-phase system with pure, highly ordered phases of P3HT and PCBM coexisting with a disordered, intimately mixed phase of P3HT and PCBM.[4−7] There is a need, therefore, for methods to control the morphology of polymer:PCBM blends in order to facilitate studies of morphological structure and device performance.

Over the last 10 years, significant efforts have been made to control the phase-separated 3D morphology of polymer:polymer blends and block copolymers using surface-directed methods. These methods are based on the preferential interaction of high surface energy polymers with high surface energy surfaces and low surface energy polymers with low surface energy surfaces. By creating a pattern with high and low surface energy domains, the morphology of a polymer blend or phase-separating block copolymer can be controlled.[8−11] Recently the interfacial composition in polymer:fullerene blends has been demonstrated to be controlled by surface energy.[12−14] The design rule that has been developed is that PCBM preferentially wets high surface energy surfaces and that P3HT preferentially wets low surface energy surfaces. This phenomenon has been reported for poly(3-alkylthiophene) (P3AT) blends with PCBM on hole transport layers,[15] has been demonstrated to affect the morphological stability of polymer:fullerene blends,[16] and was shown to be a critical factor for improved performance of inverted OPV devices relative to conventional devices.[12] However, previous efforts at extending this approach to template a 3D morphology have apparently contradicted this rule.[17]

Using microcontact printing and photolithography, Rysz and co-workers also reported the directed assembly of dielectic-polymer:conjugated-polymer blends, at the micrometer scale.[18] Employing dip-pen nanolithography, Coffey *et al.* prepared dot patterns of high surface energy domains in a low surface energy field that could direct the 3D morphology of phase-separated dielectric-polymer:conjugated-polymer blends at micrometer and submicrometer domain sizes.[17] In a subsequent paper, they demonstrated that the phase segregation of various conjugated polymer:PCBM blends could also be controlled using chemical patterns with different chemical functionalities.[19] Specifically, the patterns were found to increase or decrease the concentration of the polymer or PCBM and to lead to preferential formation of PCBM clusters. These results demonstrate that similar to the inadequacy of Flory−Huggins theory alone to explain the bulk morphology, the current design rules that were derived for surface energy directed assembly of amorphous polymer blends are inadequate for describing the nanoscale wetting behavior of semicrystalline polymer:nanoparticle blends. There is a need, therefore, to enhance understanding of the role that nanoscale wetting plays in the formation of 3D morphology of polymer:fullerene blends in order to realize a method for controlling morphology that is not dependent on an empirical optimization of kinetically controlled phase segregation. Such an approach for morphology control would enable derivation of structure−property relationships of device morphology and performance independent of polymer structure, which is currently not possible by bottom-up self-assembly.

In this study, nano-oxidation lithography (NOL) was employed to prepare chemically patterned surfaces with critical dimensions down to 50 nm in an attempt to direct the phase separation of P3HT:PCBM blends and to understand the mechanism by which directed assembly in this system occurs. Further, NOL affords patterns with little topographical contrast, thereby minimizing the effect of topography or substrate roughness on the directed assembly process. The pattern motif chosen for this study was a linear grating. Self-assembled monolayers (SAMs) with differing attachment chemistry (siloxane *vs* direct bonded) were employed in order to evaluate the potential application of direct-bonded SAMs in future studies. A combination of tapping- and contact-mode AFM studies and current-sensing AFM measurements afforded a picture of the 3D morphology of P3HT:PCBM blends atop these surface energy linear gratings.

RESULTS AND DISCUSSION

The NOL patterning method is based on the local oxidation of a SAM surface directly under a conducting AFM tip with an applied bias in the presence of water vapor.[20−22] Two different SAMs were used as the basis of the patterns prepared by NOL, one based on octyltrichlorosilane (OTS8) covalently bonded to an oxidized silicon surface and the other based on 1-dodecene (αDD) directly bonded to crystalline silicon. The OTS8 SAM was chosen based upon prior work with P3HT:PCBM on OTS8 as a surface passivation layer in OTFTs.[13] At the time of our initial experiments, NOL on direct-bonded SAMs was not known and the αDD SAM was chosen to explore the NOL process on silicon substrates bearing no native oxide layer.[23]

The slightly higher surface energy of both αDD and OTS8 SAMs relative to octadecyltrichlorosilane SAMs (OTS18) facilitated spin-casting of P3HT:PCBM blends on the substrates. However, the shorter alkyl chain length of these SAMs compared with OTS18 led to

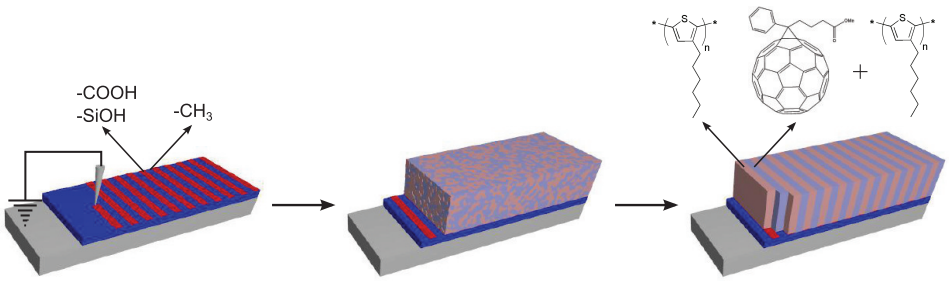

Scheme 1. Illustration of the NOL patterning, the resultant pattern chemistry (methyl or acid- and silanol-terminated), as-cast blend morphology, idealized blend morphology post-thermal treatment, and the structures of P3HT and PCBM

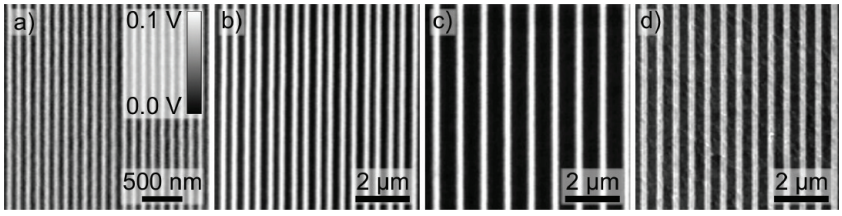

Figure 1. Contact-mode AFM images (friction data) of four chemical patterned substrates employed for this study. Patterns prepared on OTS8, OTS8-100, OTS8-300, OTS8-600 (a, b, and c), and on αDD-300 (d) illustrating the various dimensionality and small line-edge roughness of the patterned features; in all cases the vertical scale is the same.

growth of silicon oxide underneath the organic layer.[20] This was indicated by the contact-mode AFM images of the patterns where the patterned regions appeared to be raised about 1−2 nm above the field. The oxide growth may have compromised the structural integrity of the SAM, and, as a result, the patterned regions presented carboxylic and silanol groups. Due to the higher surface energy of both carboxylic and silanol groups compared with the native methyl-terminated SAM, the patterns appeared as areas of enhanced friction (bright) in the friction-force AFM images shown in Figure 1. Since the role of surface energy contrast, and not specific chemical functionality, was the focus of this study, the apparent chemical heterogeneity of the high surface energy domains was not of concern going forward. The patterns on OTS8 were prepared with nominal pitches (combination of the acid-terminated line width and the methyl-terminated line space between features)[24] of 100, 300, and 600 nm (and are referred to below as OTS8-100, OTS8-300, and OTS8-600; see Figure 1a, b, and c, respectively). For OTS8-100 the nominal line width and line spacing were both 50 nm, while for the remaining OTS8 patterns a constant acid-terminated domain line width (approximately 200 nm) and varying methyl-terminated line spaces (200 to 400 nm) were prepared. The varying methyl-terminated line spaces were chosen to facilitate differentiating between the blend film domains formed during directed assembly. Furthermore, the use of patterns with varying domain width enabled studies of the effect of template size and periodicity on the morphology of the phase-separated blends. This provided insight into the mechanism of directed assembly (nucleation and growth or spinodal decomposition).[25,26] The pattern on αDD was prepared with a pitch of 300 nm (and referred to as αDD-300; see Figure 1d). All the grating patterns employed in this study had small line-width roughness (lateral variations in the width of the patterned features over the length of the feature).[24] Blend films were spun onto the various chemical patterns using a solution composed of a 1:1 weight ratio of P3HT to PCBM at a total solids concentration of 1 wt % in chloroform, and the resulting topography and lateral morphology were investigated using a combination of AFM methods. The 1:1 (by weight) blend ratio was chosen to replicate the optimal blend ratio for P3HT:PCBM OPV devices.[27] The selection of chloroform as the solvent was made since its low surface tension enabled good wetting of the low surface energy SAM, while it maintained good solubility of P3HT and PCBM. Films processed from chloroform are homogeneous (phase separation between the PCBM and P3HT was arrested by rapid film drying) due to the miscibility of the two components in chloroform solution.[28] These properties facilitated the study of the directed-assembly mechanism on both as-cast and thermally treated films. The spin recipe utilized in these studies resulted in films of consistent appearance and thickness (50 nm as measured by ellipsometry). No significant contrast in the friction images was observed for these films, consistent with the small difference in surface energy between P3HT and PCBM (<10 mN/m).

Contact-mode AFM (CM-AFM) studies revealed relatively smooth films (rms roughness ≤1 nm) for the as-cast blend films on unpatterned substrates (Figure 2a). The film spun atop the OTS8-100 patterned substrate appeared similar to the unpatterned control (Figure 2b), indicating that at this pitch no surface-directed assembly

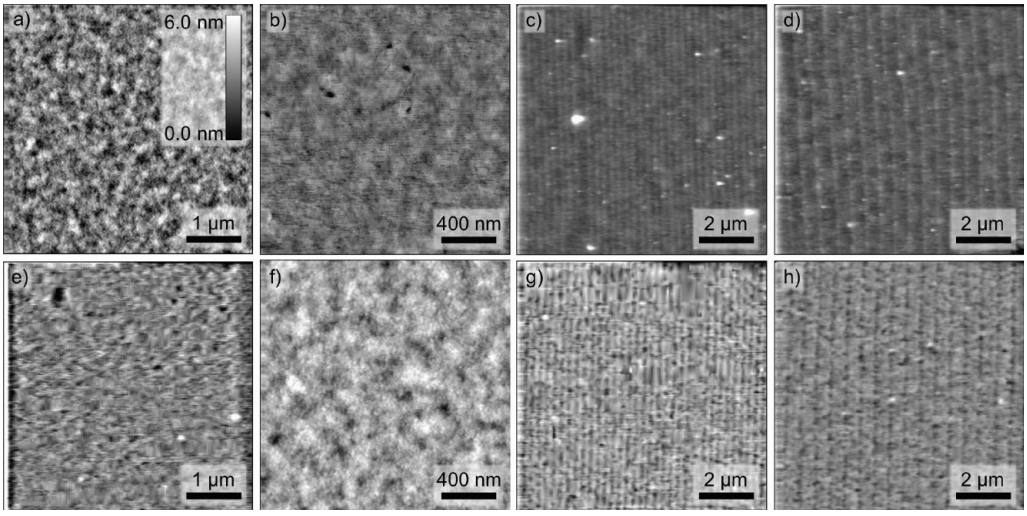

Figure 2. CM-AFM images of the as-cast P3HT:PCBM blend films spun atop an unpatterned OTS8 control substrate (a), OTS100 (b), OTS-300 (c), and OTS-600 (d) substrates. Post-thermal treatment topography of the films atop an unpatterned OTS8 control substrate (e), OTS100 (f), OTS-300 (g), and OTS-600 (h) substrates. For all images, the vertical scale is the same.

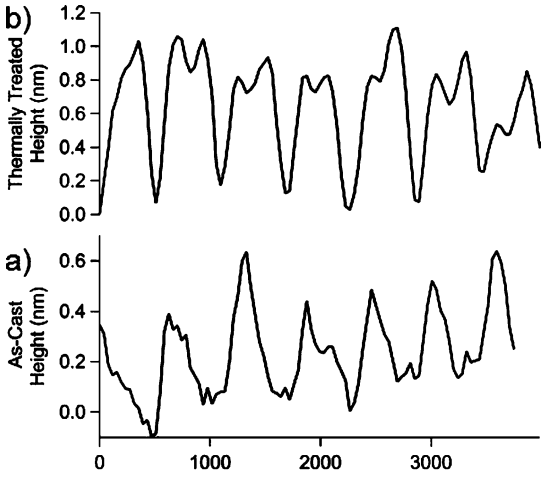

Figure 3. CM-AFM profiles of the P3HT:PCBM as-cast blend atop OTS8-600 (a) and P3HT:PCBM thermally treated atop the OTS8-600 film (b).

occurred. For films spun on patterns with features larger than 100 nm the as-cast blend films possessed raised lines (see Figure 2c, d). The lines are approximately 1−2 nm in height, as shown by the cross-sectional profile of the sample in Figure 2d (shown in Figure 3a). The raised lines were similar to the line width and height of the acid-terminated domains with a pitch comparable to that of the underlying pattern. Several effects may contribute to this behavior. The observed topography may result from conformal coating of the underlying topography of the pattern, as observed for the casting of polymer films onto micrometer-scale patterns.[29,30] Moreover, Marangoni-like fluid flow induced by either surface chemical gradients[31,32] or solvent-concentration gradients through the film during the evaporation[33] may also contribute to the as-cast film topography. Similar topographic variations on the nanometer scale were also

TABLE 1. Pitch and Feature Width Data for Blend Films on Patterned Substrates

sample	pitch pattern (±10 nm)[c]	pitch as-cast (±10 nm)[d]	pitch thermally treated (±10 nm)
OTS8-100	100	N/A	N/A
OTS8-300	295	288	296
OTS8-600	584	575	601
αDD-300 TM[a]	241	250	237
αDD-300 CM[b]	241	256	243
αDD-800 TM	760	823	738
αDD-800 CM	760	722	794

[a] TM indicates tapping mode. [b] CM indicates contact mode. [c] From friction data of the patterned film. [d] From topography data of the blend films.

observed by Ginger and co-workers for as-cast polymer: fullerene blends on micrometer-scale chemical patterns that exhibited nanometer scale topography.[19] Subsequent thermal treatment (130 °C for 20 min) resulted in unexpected changes to the as-cast topography for films atop the OTS-300 and OTS-600 patterns, but not for films atop the OTS-100 pattern (see Figure 2f, g, and h and Figure 3). In contrast, the control sample (Figure 2e) and the OTS8-100 sample (Figure 2f) showed no significant changes in the topography upon thermal annealing. For the OTS-300 and OTS-600 patterns the initial vertical topography of the as-cast films inverted during thermal treatment. Specifically, the previously raised lines of the as-cast films atop the acid-terminated domains appeared as recessed lines after thermal treatment. The depth of the recessed lines was approximately 1 nm, and the width of the lines remained consistent with the width of the acid-terminated domains and the as-cast, raised lines (Figure 3b). Furthermore, the pitch of the observed topographic features in the OTS8-300 and OTS8-600 did not change significantly upon thermal treatment despite

the observed changes in vertical topography, indicating that the observed change in topography reflected the changes in 3D morphology and that the process of 3D-morphology evolution was directed by the underlying chemical pattern (Figure 2g and h and Table 1).

As illustrated in Figure 4, similar behavior was observed for blend films spun atop an αDD pattern with a similar characteristic length to the OTS8-300 template. Additional tapping-mode AFM (TM-AFM) height measurements (Figure 4a) on the same samples revealed similar topographical features as obtained with CM-AFM measurements (Figure 4b). To further compare the two methods, the power spectral density function of linear profiles perpendicular to the long axis of the lines (Figure 4c) illustrated good agreement (Table 1). Phase data from the tapping-mode measurements did not exhibit an observable phase contrast that could be correlated with the observed topography, which demonstrated the necessity for an alternative method for probing the composition of the observed topographic features.[34,35] The observed agreement between the TM-AFM and CM-AFM topography results are particularly relevant since the subsequent current-sensing measurements were made in contact mode and therefore required that the CM-AFM imaging accurately reproduced the underlying topography without damaging the film during scanning.

No microscopic crystals of PCBM were observed under these thermal treatment conditions (130 °C) on both the patterned and the control samples. These results differ from those of Ginger and co-workers, who observed that the features on the high surface energy domains ripened into structures that were raised above the field of the film and resembled PCBM crystals.[19] This difference can be partly reconciled by the differing weight ratio of PCBM to P3HT employed in that study (2:1) *versus* the ratio (1:1) in the present study. By using a higher ratio of PCBM to P3HT, an excess of PCBM would be available to promote the formation of PCBM crystals by the initial phase-separated morphology. In a separate work, He *et al*. reported that the substrate−film interfacial composition plays a significant role in the formation of PCBM crystals in blend films. In that work, PCBM crystal growth below the glass transition of PCBM (<150 °C) was observed for films cast upon high surface energy substrates, compared to low surface energy substrates, where the formation of PCBM crystals required significantly higher temperatures (180 °C).[16] The suppression of PCBM crystallization observed here is likely due to a combination of interfacial and bulk effects. In the bulk of the film, the highly homogeneous and well-dispersed blend morphology undoubtedly results in a system with a small number of crystal seeds, thereby suppressing crystallization in the bulk.[16,36] In the system under study here the OTS8 SAM−blend film interface was expected to be rich in P3HT,[14,15,37] which

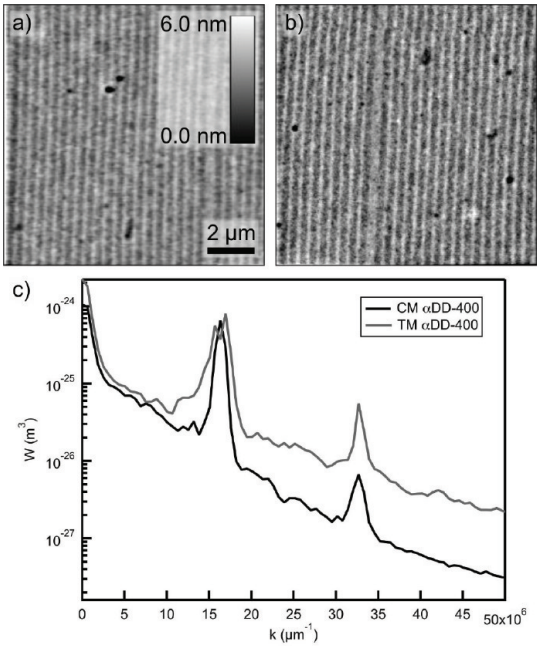

Figure 4. Contact- (a) and tapping-mode (b) images of thermally treated blend films atop the αDD-300 patterned substrate and the comparison of the power spectral density function of a line profile through each image illustrating the similarity between the two images. The horizontal and vertical scales are identical for (a) and (b).

would inhibit PCBM crystallization at the substrate−film interface similar to what was observed for P3HT:PCBM blend films deposited on PEDOT:PSS.[16] In order to confirm that the observed topographic patterns are representative of bulk morphology, measurements sensitive to the compositional inhomogeneity of the blend films were necessary in order to show that the observed topography was due to the formation of localized domains of PCBM and P3HT.

Current-sensing AFM (C-AFM) was employed as a measurement sensitive to the bulk film composition by virtue of the differing charge transport of PCBM and P3HT. C-AFM probed the average conductivity through the film, which was dependent on the local composition of the film (*i.e.*, the vertical composition). These studies are complementary to the topography mapping by contact- and tapping-mode AFM and allow mapping of the P3HT:PCBM blend film morphology as directed by the underlying chemical pattern. In our experiments, the tip was grounded and the current flowing through the tip as a function of a bias applied to the substrate was recorded simultaneously with topography images. Contrast between domains was based upon the Fermi level of the conductive AFM tip and the HOMO and LUMO levels of P3HT and PCBM. By using a platinum AFM tip with a Fermi level better aligned with the HOMO of P3HT than with the HOMO of PCBM, and measuring the samples in the dark under a N_2 atmosphere with low humidity (<1%), this system effectively collected holes and did not chemically

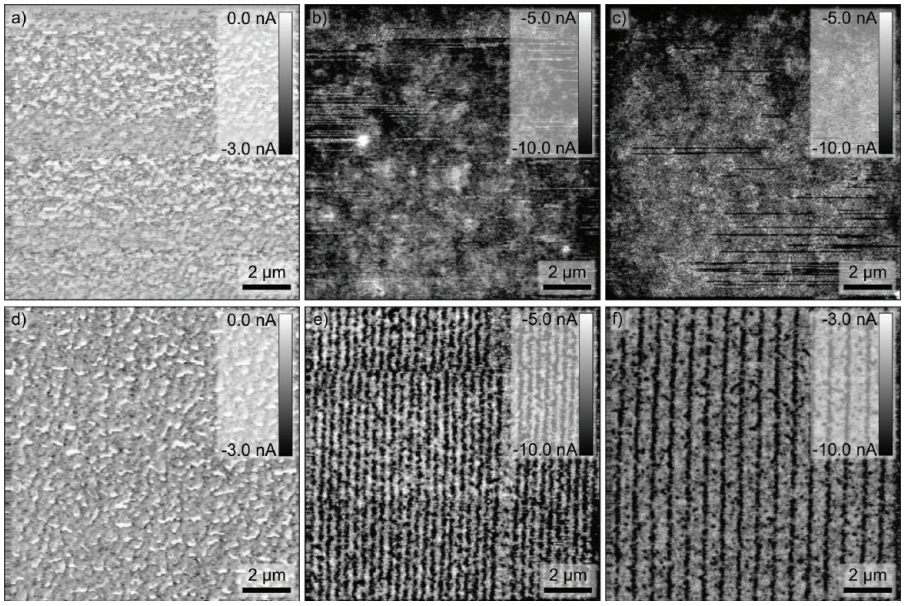

Figure 5. Current-sensing AFM images of P3HT (a, d) and P3HT:PCBM (b, c, e, and f) blend films on patterned substrates illustrating the formation of a 3D morphology in the blend films (e, f) post-thermal treatment. The underlying pattern for a, d and c, f was OTS8-600 and that for b, e was OTS8-300. All data were collected at a substrate bias of −8 V.

oxidize the P3HT:PCBM blend film.[38] No degradation of the film was detected in topographic or current-sensing images of the previously imaged areas, similar to results reported by Hamadani and Dante.[35,39] The contrast between hole and electron collection was further enhanced by the high mobility of holes in P3HT *versus* holes or electrons in PCBM.[35] Under these assumptions, regions of higher current in the C-AFM images at negative bias correspond to P3HT-rich domains.

Representative C-AFM images recorded at negative bias for as-cast and thermally treated films are shown in Figure 5. These data have been recorded using biases that are large enough (−8 V) for the carrier to tunnel through the underlying silicon oxide layer. The images of the as-cast P3HT (5a) and P3HT:PCBM blend (5b, c) films with a −8 V substrate bias exhibit transport of current (holes) that was heterogeneous across the imaged area with localized domains of high and low current not correlated with the underlying chemical patterns. These results are consistent with those reported for P3HT:PCBM blends atop unpatterned substrates where contact asymmetry, local composition, ordering defects, and surface effects resulted in a heterogeneous distribution of current transport.[35,38,40,41] Upon thermal treatment, a line-grating pattern of high (bright) and low current (dark) was observed that correlated with the observed topography (see Figure 6) and the underlying patterned template (see Figure 5e and f). Comparing the OTS8-600 (Figure 1c) chemical pattern and the thermally treated blend film (Figure 5f) the areas of high current correspond to P3HT-rich domains, consistent with the oxidized lines of the underlying patterns, and areas of low current correspond to PCBM-rich domains, consistent with the methyl-terminated line spaces of the underlying pattern. Furthermore, Figure 5e and f show that the P3HT-rich domains are not uniform and the domain boundaries are not as sharp as the underlying chemical patterns. Bright, P3HT-rich spots are also visible, albeit in smaller number, on the methyl-terminated regions of the pattern. These results indicate that the pattern fidelity of P3HT:PCBM blend films upon the chemical patterns is imperfect. Images obtained at positive biases (up to 10 V) showed little contrast and few current levels and consequently are not reported here.

The observed patterns in the C-AFM reflect variations in the bulk conductivity of the film rather than interfacial effects due, for example, to injection barriers at the substrate/blend and blend/air interfaces. Although differences in the SAM surface composition and the slightly thicker oxide layer under the acid-terminated domains could act as injection barriers, in practice this possibility is ruled out by C-AFM studies of pure P3HT control films on patterned substrates (Figure 5a and d). These data exhibit no pattern in either topography or current images, demonstrating that the underlying pattern is not the source of the observed current images in the blend films. Pure PCBM films could not be cast on these substrates using the same spin conditions as for the blend or P3HT control films. This is due to the higher surface energy of PCBM relative to the methyl-terminated SAM. It is also unlikely that the P3HT-enriched layer at the blend/air interface contributes significantly to the pattern seen in the C-AFM images of the blend films. Although this "wetting layer" was shown to limit charge collection in photocurrent AFM measurements conducted in the open circuit voltage condition, this effect is unimportant at the larger bias used here (−8 V), where charge

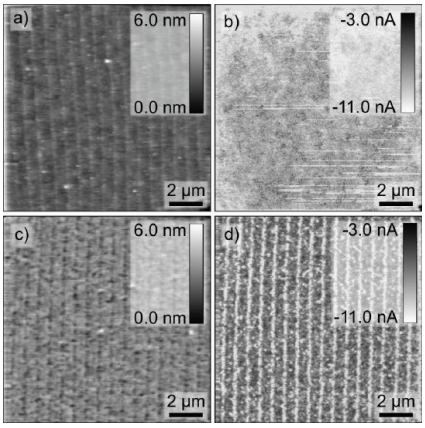

Figure 6. Comparison of height (a and c) and current (b and d) for the same areas of the as-cast (a and b) and thermally treated (c and d) blend film atop the OTS8-600 pattern demonstrating the correlation of high-current areas with the topography in the thermally treated case.

injection contributes predominantly to the measured current.

The C-AFM results reported here are consistent with the three-phase system model for P3HT:PCBM blend films (pure P3HT, pure PCBM, and mixed amorphous phase).[4,42] High current was observed for the domains on the acid-terminated lines, consistent with a semicrystalline (higher mobility) P3HT-rich phase. The domains on the methyl-terminated spaces exhibited a lower background current, indicative of a PCBM-rich phase that contained a significant amount of amorphous P3HT. The topography data for the thermally treated films further support this result, as the features atop the methyl-terminated spaces are taller than the domains atop the acid-terminated lines, suggesting that the bulk of the material is still in some combination of pure and mixed phases atop the methyl-terminated domains.

Upon first glance, these results seem inconsistent with earlier studies of interfacial segregation for polymer:fullerene blends, namely, that the high surface energy component (PCBM) preferentially wets high surface energy substrates.[13,14,43] In this study, however, the lower surface energy component (P3HT) segregates on the high surface energy features (oxidized lines). These results are rationalized as follows. The absence of template-directed phase separation in the as-cast films (Figure 5b and c) results from the specific processing conditions used here. Due to the rapid drying of the solvent (chloroform *vs* chloro- or dichlorobenzene used in past studies), the blend components may not have had enough time to interact with the substrate in order to induce surface-energy-driven phase segregation at the solution−substrate interface. Similar behavior has been observed for phase-segregating polymer blends, where decreasing interaction time between a patterned substrate and a blend solution decreased the as-cast pattern fidelity.[44] The observed topographic contrast therefore likely arises from both substrate roughness[29,30] and Marangoni-like fluid flow induced by substrate chemical gradients.[31,32]

Due to the kinetic arresting of the phase separation, thermal treatment was applied to the film to provide enhanced mobility of the polymer, and this resulted in phase segregation to a more favorable energy configuration, with P3HT preferentially wetting the acid-terminated domains. The chemical gradients occurring at the boundary between the high- and low-energy domains give rise to a lateral force (Marangoni-like effect) on the uniformly distributed as-cast polymer film, and this is responsible for the observed template-directed phase separation.[31,45] Similar behavior has been reported for systems involving the directed assembly of P3HT.[17−19] In a report from Ginger and co-workers[17] using templates with high surface energy features in a low surface energy field on the same length scale as those used here (<300 nm), the lower surface energy P3HT (26.9 mN/m)[46] preferentially wet the high surface energy features when deposited from a solution with polystyrene (30.5 mN/m).[47] For micrometer-scale features, Rysz and co-workers also observed that polystyrene preferentially wets low surface energy domains.[18] However, unlike for P3HT and polystyrene, P3HT and PCBM are miscible, and therefore, the fidelity of the template-directed phase separation is not very high, as indicated by the presence of "defects" in the C-AFM data of the annealed films. This can be understood when considered in the context of several recent studies.[4−7,42] Pulse-diffusion NMR experiments have demonstrated that even upon extensive annealing above the glass transition of PCBM and the melting transition of P3HT, a significant portion of PCBM remains dispersed within a P3HT matrix.[7] Dadmun and co-workers have determined an upper bound on the miscibility of PCBM in P3HT of 20% based upon SANS measurements.[42] Calorimetry, scattering, and TOF-SIMS studies have resulted in the determination of a χ parameter of −0.3, indicating that PCBM and P3HT are miscible.[6] These previous studies suggest that even in the best case scenario a small fraction of the PCBM present in the blend remains highly dispersed in P3HT and that it may be possible for localized PCBM domains to form within a P3HT domain or *vice versa*.[4,5,42]

The absence of template-directed phase segregation for pattern pitches smaller than ~100 nm suggests that the morphology forming mechanism is analogous to the surface-directed spinodal decomposition scenario in polymer blends.[8,10,25,48] In these systems, the inherent domain scale D increases during thermal annealing and the best pattern-directed phase separation is achieved if D is comparable to the pattern periodicity λ. However, if $\lambda \ll D$, the pattern has little effect on the phase separation. In the case of the OTS8-100 patterns the inherent P3HT domain size is larger than the width of the carboxylic lines (50 nm), resulting in poor pattern replication.

These results make clear that the phase segregation of P3HT:PCBM blends is more complex than that of polymer blends, and while a rigorous reworking of the relevant theory is beyond the scope of this work, we can point to several critical issues beyond the miscibility of the blend components and their relative surface energies that will need to be addressed in the future based upon the work reported here and those previously published.[17,19] The roles of the solvent and the template-domain surface energies appear to be critical. The physical shape of the components (*i.e.*, sphere, rigid-rod) and the phase behavior (amorphous, condis crystal, *etc.*) also are important parameters to consider since they vary widely from material to material.[49] Additionally, the bulk behavior of the blend has to be addressed, as it has recently been demonstrated by several groups that subtle changes to the solubilizing side-chain density, attachment location, and structure can result in changes in the behavior of conjugated polymer:fullerene blends. These changes range from altering the backbone linearity,[50,51] to the polymer packing,[52−56] to the polymer:fullerene packing.[57] All of these potentially applicable parameters of surface-directed spinodal decomposition theory have been demonstrated to be energetically relevant to the bulk behavior of conjugated polymer:fullerene blends, and we are pursuing avenues of exploration to further understand this complicated phase space at the current time.

CONCLUSIONS

Nano-oxidation lithography of SAMs has been employed to prepare nanometer-scale chemical templates to direct the assembly of a 3D morphology for P3HT:PCBM blends. These templates, consisting of alternating lines of high surface energy carboxylic acid and low surface energy methyl groups, were found to be effective at directing the assembly down to features of approximately 200 nm in width for films with a consistent thickness, but did not direct the assembly at feature sizes of smaller dimensions. The observed morphology consisted of P3HT domains atop acid-terminated domains with a mixed phase of pure PCBM and an intimately mixed, amorphous P3HT:PCBM blend atop the methyl-terminated spaces. These results are consistent with a directed spinodal decomposition mechanism for the formation of the morphology. These results also demonstrate that directing the lateral dimensionality of domains on the order of the exciton diffusion length for P3HT (∼20 nm) represents an intriguing and scientifically challenging goal.

METHODS AND MATERIALS

Octyltrichlorosilane (99%, Gelest), hexadecane (99%, Aldrich), chloroform (HPLC grade, Aldrich), and 2-propanol (HPLC grade, Aldrich) were used as received without additional purification. Water was purified using a Millipore purification system. P3HT ($M_w \approx 50\,000$ g·mol^{-1}, PDI ≈ 1.7, regioregularity > 95%, Reike) and PCBM (>99% purity, Nano-C) were used as received. Silicon wafers were prime grade, ⟨100⟩ or ⟨111⟩ orientation, boron-doped to 0.01−0.02 ohm/cm, and were used as received from WRS Materials. Silver paste (SPI) was used as received. Teflon-capped vials, PET pipet tips, syringes, and 0.45 μm PTFE syringe filters were used as received from Thermo-Fischer. Ultrapure N_2 (Brookhaven National Lab) and supercritical CO_2 (Praxair) were used as received.

All wafers were cleaned by employing the following procedure: (a) 10 min UV ozone exposure, (b) water wash, and (c) N_2 dry. All wafers were coated within 5 min of cleaning to minimize contamination by adventitious carbon. Siloxane-based self-assembled monolayers were prepared on Si ⟨100⟩ by immersing a freshly cleaned Si wafer into a 2 mM solution of octyltrichlorosilane in hexadecane in an oven-dried amber flask. The flask was capped with a Teflon-lined lid and then placed in the dark overnight. The wafers were then removed and washed by sequential sonication in chloroform, 2-propanol, and water. SAM formation was confirmed by water contact angle measurements (Θ_w = 105°). Direct-bonded SAMS were prepared on hydrogen-passivated Si ⟨111⟩ using 1-dodecene as previously described.[58]

Nano-oxidation lithography was performed by placing a 1 cm^2 silicon substrate with a SAM onto the stage of an Agilent 5500 AFM system equipped with a closed-loop scanner. Electrical contact to the wafer was made by attaching a platinum wire to the surface with silver paste and confirmed with a multimeter prior to placement in the controlled environment chamber. Once the stage was mounted, the controlled environment chamber was sealed and humid N_2 was flowed into the chamber until the relative humidity of the chamber was between 85% and 95%. Humidity was controlled by a home-built PID controller system. Platinum-coated conductive tips for contact-mode AFM (CSC17 Pt/Ti Mikromasch) were used to write well-defined patterns using the Picolith functionality of the PicoView software with the write speed and applied bias controlled to maximize surface oxidation while minimizing SAM degradation and silanol formation. All patterns were written in relation to a macroscopic fiducial mark in order to facilitate identification of the pattern location after film deposition.

Solutions of P3HT and P3HT:PCBM were prepared and subsequently deposited onto substrates in an Ar-purged glovebox maintained at less than 5 ppm O_2 (Omni model, Vacuum Atmospheres Corp., Hawthorne, CA, USA). P3HT and P3HT:PCBM blend solutions were prepared at 1 wt % in chloroform and were stirred overnight at 60 °C, then cooled to room temperature prior to use. All solutions were used within 1 month of preparation. P3HT:PCBM blend films were prepared by deposition of a 1 wt % solution of P3HT and PCBM (1:1 w/w) through a 0.45 μm filter onto patterned substrates previously cleaned with supercritical CO_2. All films were formed by spin-casting at 1000 rpm for 60 s, at the maximum acceleration setting, using a Laurell Technologies Corporation (North Wales, PA, USA) model WS-650 Hz-23 spin coater. P3HT and blend films on unpatterned substrates were deposited under identical conditions to those on patterned substrates. Thermal treatment was conducted in an oven at 130 °C under dynamic vacuum for 20 min, followed by quenching on a block of aluminum at 25 °C.

Tapping- and contact-mode AFM measurements were made using the same AFM system employed for NOL patterning. Tapping-mode measurements were made with silicon AFM tips (Tap300Al-G, Budget Sensors) with a resonant frequency of 300 kHz and a force constant of 40 N/m. Contact-mode measurements were made with silicon tips (ContAl-G, Budget Sensors) with a resonant frequency of 13 kHz and a force constant of 0.2 N/m. Current-sensing (C-AFM) measurements were also

made using the Agilent 5500 AFM system and employing the same tips as used for patterning. In order to minimize any possibility of chemical oxidation from oxygen radicals or water that might be generated during C-AFM imaging, the controlled environment chamber was purged with dry N_2 for a minimum of 20 min prior to measurements being performed, and all measurements were made below 5% relative humidity. In all cases, topography, friction, and current images were collected simultaneously, and a final topography and friction image pair was collected after the C-AFM scans to ensure that no changes to the surface occurred during C-AFM imaging.

Conflict of Interest: The authors declare no competing financial interest.

Acknowledgment. This research was supported by the U.S. Department of Energy, Office of Basic Energy Sciences, Materials Sciences and Engineering Division, under Contract No. DE-AC02-98CH10886. Part of the research was carried out at the Center for Functional Nanomaterials, Brookhaven National Laboratory, which is supported by the U.S. Department of Energy, Office of Basic Energy Sciences, under Contract No. DE-AC02-98CH10886. The authors also wish to thank B. Hammadani and C. K. Chan for helpful discussions regarding interpretation of the current-sensing AFM data.

REFERENCES AND NOTES

1. He, F.; Yu, L. How Far Can Polymer Solar Cells Go? In Need of a Synergistic Approach. *J. Phys. Chem. Lett.* **2011**, *2*, 3102–3113.
2. Segalman, R. A.; McCulloch, B.; Kirmayer, S.; Urban, J. J. Block Copolymers for Organic Optoelectronics. *Macromolecules* **2009**, *42*, 9205–9216.
3. Wu, W.-R.; Jeng, U.-S.; Su, C.-J.; Wei, K.-H.; Su, M.-S.; Chiu, M.-Y.; Chen, C.-Y.; Su, W.-B.; Su, C.-H.; Su, A.-C. Competition between Fullerene Aggregation and Poly(3-Hexylthiophene) Crystallization upon Annealing of Bulk Heterojunction Solar Cells. *ACS Nano* **2011**, *5*, 6233–6243.
4. Erb, T.; Zhokhavets, U.; Gobsch, G.; Raleva, S.; Stühn, B.; Schilinsky, P.; Waldauf, C.; Brabec, C. J. Correlation between Structural and Optical Properties of Composite Polymer/Fullerene Films for Organic Solar Cells. *Adv. Funct. Mater.* **2005**, *15*, 1193–1196.
5. Treat, N. D.; Brady, M. A.; Smith, G.; Toney, M. F.; Kramer, E. J.; Hawker, C. J.; Chabinyc, M. L. Interdiffusion of PCBM and P3HT Reveals Miscibility in a Photovoltaically Active Blend. *Adv. Energy Mater.* **2010**, *1*, 82–89.
6. Chen, D.; Nakahara, A.; Wei, D.; Nordlund, D.; Russell, T. P. P3HT/PCBM Bulk Heterojunction Organic Photovoltaics: Correlating Efficiency and Morphology. *Nano Lett.* **2011**, *11*, 561–567.
7. Nieuwendaal, R. C.; Ro, H.-W.; Germack, D. S.; Kline, R. J.; Toney, M. F.; Chan, C. K.; Acrawal, A.; Gundlach, D. J.; VanderHart, D. L.; Delongchamp, D. M. Measuring Domain Sizes and Compositional Heterogeneities in P3HT-PCBM Bulk Heterojunction Thin Films with 1H Spin Diffusion NMR Spectroscopy. *Adv. Funct. Mater.* **2012**, *22*, 1255–1266.
8. Böltau, M.; Walheim, S.; Mlynek, J.; Krausch, G.; Steiner, U. Surface-Induced Structure Formation of Polymer Blends on Patterned Substrates. *Nature* **1998**, *391*, 877–879.
9. Kim, S. O.; Solak, H. H.; Stoykovich, M. P.; Ferrier, N. J.; de Pablo, J. J.; Nealey, P. F. Epitaxial Self-Assembly of Block Copolymers on Lithographically Defined Nanopatterned Substrates. *Nature* **2003**, *424*, 411–414.
10. Raczkowska, J.; Bernasik, A.; Budkowski, A.; Rysz, J.; Gao, B.; Lieberman, M. Compositional Mismatch between Chemical Patterns on a Substrate and Polymer Blends Yielding Spin-Cast Films with Subpattern Periodicity. *Macromolecules* **2007**, *40*, 2120–2125.
11. Xu, J.; Park, S.; Wang, S.; Russell, T. P.; Ocko, B. M.; Checco, A. Directed Self-Assembly of Block Copolymers on Two-Dimensional Chemical Patterns Fabricated by Electro-Oxidation Nanolithography. *Adv. Mater.* **2010**, *22*, 2268–2272.
12. Xu, Z.; Chen, L.-M.; Yang, G.; Huang, C.-H.; Hou, J.; Wu, Y.; Li, G.; Hsu, C.-S.; Yang, Y. Vertical Phase Separation in Poly(3-Hexylthiophene): Fullerene Derivative Blends and Its Advantage for Inverted Structure Solar Cells. *Adv. Funct. Mater.* **2009**, *19*, 1227–1234.
13. Germack, D. S.; Chan, C. K.; Hamadani, B. H.; Richter, L. J.; Fischer, D. A.; Gundlach, D. J.; Delongchamp, D. M. Substrate-Dependent Interface Composition and Charge Transport in Films for Organic Photovoltaics. *Appl. Phys. Lett.* **2009**, *94*, 233303.
14. Rice, A. H.; Giridharagopal, R.; Zheng, S. X.; Ohuchi, F. S.; Ginger, D. S.; Luscombe, C. K. Controlling Vertical Morphology within the Active Layer of Organic Photovoltaics Using Poly(3-Hexylthiophene) Nanowires and Phenyl-C61-Butyric Acid Methyl Ester. *ACS Nano* **2011**, *5*, 3132–3140.
15. Germack, D. S.; Chan, C. K.; Kline, R. J.; Fischer, D. A.; Gundlach, D. J.; Toney, M. F.; Richter, L. J.; Delongchamp, D. M. Interfacial Segregation in Polymer/Fullerene Blend Films for Photovoltaic Devices. *Macromolecules* **2010**, *43*, 3828–3836.
16. He, C.; Germack, D. S.; Kline, R. J.; Delongchamp, D. M.; Fischer, D. A.; Snyder, C. R.; Toney, M. F.; Kushmerick, J. G.; Richter, L. J. Influence of Substrate on Crystallization in Polythiophene/Fullerene Blends. *Sol. Energy Mater. Sol. Cells* **2011**, *95*, 1375–1381.
17. Coffey, D. C.; Ginger, D. S. Patterning Phase Separation in Polymer Films with Dip-Pen Nanolithography. *J. Am. Chem. Soc.* **2005**, *127*, 4564–4565.
18. Jaczewska, J.; Budkowski, A.; Bernasik, A.; Raptis, I.; Moons, E.; Goustouridis, D.; Haberko, J.; Rysz, J. Ordering Domains of Spin Cast Blends of Conjugated and Dielectric Polymers on Surfaces Patterned by Soft- and Photo-Lithography. *Soft Matter* **2008**, *5*, 234–241.
19. Park, L. Y.; Munro, A. M.; Ginger, D. S. Controlling Film Morphology in Conjugated Polymer:Fullerene Blends with Surface Patterning. *J. Am. Chem. Soc.* **2008**, *130*, 15916–15926.
20. Maoz, R.; Cohen, S. R.; Sagiv, J. Nanoelectrochemical Patterning of Monolayer Surfaces: Toward Spatially Defined Self-Assembly of Nanostructures. *Adv. Mater.* **1999**, *11*, 55–61.
21. Hoeppener, S.; Schubert, U. S. Fabrication via Electrochemical Oxidation of Self-Assembled Monolayers and Site-Selective Derivatization of Surface Templates. *Small* **2005**, *1*, 628–632.
22. Cai, Y.; Ocko, B. M. Electro Pen Nanolithography. *J. Am. Chem. Soc.* **2005**, *127*, 16287–16291.
23. Martinez, R. V.; Chiesa, M.; Garcia, R. Nanopatterning of Ferritin Molecules and the Controlled Size Reduction of Their Magnetic Cores. *Small* **2011**, *7*, 2914–2920.
24. Mack, C. A. *Field Guide to Optical Lithography*; SPIE Press: Bellingham, WA, 2006.
25. Jones, R. A. L.; Norton, L. J.; Kramer, E. J.; Bates, F. S.; Wiltzius, P. Surface Directed Spinodal Decomposition. *Phys. Rev. Lett.* **1991**, *66*, 1326–1329.
26. Nisato, G.; Ermi, B. D.; Douglas, J. F.; Karim, A. Excitation of Surface Deformation Modes of a Phase-Separating Polymer Blend on a Patterned Substrate. *Macromolecules* **1999**, *32*, 2356–2364.
27. Li, G.; Shrotriya, V.; Huang, J.; Yao, Y.; Moriarty, T.; Emery, K.; Yang, Y. High-Efficiency Solution Processable Polymer Photovoltaic Cells by Self-Organization of Polymer Blends. *Nat. Mater.* **2005**, *4*, 864–868.
28. Verploegen, E.; Mondal, R.; Bettinger, C. J.; Sok, S.; Toney, M. F.; Bao, Z. Effects of Thermal Annealing upon the Morphology of Polymer-Fullerene Blends. *Adv. Funct. Mater.* **2010**, *20*, 3519–3529.
29. Huang, X. D.; Bao, L. R.; Cheng, X.; Guo, L. J.; Pang, S. W.; Yee, A. F. Reversal Imprinting by Transferring Polymer from Mold to Substrate. *J. Vac. Sci. Technol. B* **2002**, *20*, 2872–2876.
30. Daoulas, K. C.; Müller, M.; Stoykovich, M. P.; Kang, H.; de Pablo, J. J.; Nealey, P. F. Directed Copolymer Assembly on Chemical Substrate Patterns: a Phenomenological and Single-Chain-in-Mean-Field Simulations Study of the

Influence of Roughness in the Substrate Pattern. *Langmuir* **2008**, *24*, 1284–1295.
31. Konnur, R.; Kargupta, K.; Sharma, A. Instability and Morphology of Thin Liquid Films on Chemically Heterogeneous Substrates. *Phys. Rev. Lett.* **2000**, *84*, 931–934.
32. Kargupta, K.; Konnur, R.; Sharma, A. Spontaneous Dewetting and Ordered Patterns in Evaporating Thin Liquid Films on Homogeneous and Heterogeneous Substrates. *Langmuir* **2001**, *17*, 1294–1305.
33. Heriot, S. Y.; Jones, R. A. L. An Interfacial Instability in a Transient Wetting Layer Leads to Lateral Phase Separation in Thin Spin-Cast Polymer-Blend Films. *Nat. Mater.* **2005**, *4*, 782–786.
34. Coffey, D. C.; Reid, O. G.; Rodovsky, D. B.; Bartholomew, G. P.; Ginger, D. S. Mapping Local Photocurrents in Polymer/Fullerene Solar Cells with Photoconductive Atomic Force Microscopy. *Nano Lett.* **2007**, *7*, 738–744.
35. Hamadani, B. H.; Gergel-Hackett, N.; Haney, P. M.; Zhitenev, N. B. Imaging of Nanoscale Charge Transport in Bulk Heterojunction Solar Cells. *J. Appl. Phys.* **2011**, *109*, 124501.
36. Bull, T. A.; Pingree, L. S. C.; Jenekhe, S. A.; Ginger, D. S.; Luscombe, C. K. The Role of Mesoscopic PCBM Crystallites in Solvent Vapor Annealed Copolymer Solar Cells. *ACS Nano* **2009**, *3*, 627–636.
37. Chen, L.-M.; Xu, Z.; Hong, Z.; Yang, Y. Interface Investigation and Engineering – Achieving High Performance Polymer Photovoltaic Devices. *J. Mater. Chem.* **2010**, *20*, 2575–2598.
38. Alexeev, A.; Loos, J.; Koetse, M. M. Nanoscale Electrical Characterization of Semiconducting Polymer Blends by Conductive Atomic Force Microscopy (C-AFM). *Ultramicroscopy* **2006**, *106*, 191–199.
39. Dante, M.; Peet, J.; Nguyen, T. Q. Nanoscale Charge Transport and Internal Structure of Bulk Heterojunction Conjugated Polymer/Fullerene Solar Cells by Scanning Probe Microscopy. *J. Phys. Chem. C* **2008**, *112*, 7241–7249.
40. Dante, M.; Peet, J.; Nguyen, T. Q. Nanoscale Charge Transport and Internal Structure of Bulk Heterojunction Conjugated Polymer/Fullerene Solar Cells by Scanning Probe Microscopy. *J. Phys. Chem. C* **2008**, *112*, 7241–7249.
41. Pingree, L. S. C.; Reid, O. G.; Ginger, D. S. Imaging the Evolution of Nanoscale Photocurrent Collection and Transport Networks during Annealing of Polythiophene/Fullerene Solar Cells. *Nano Lett.* **2009**, *9*, 2946–2952.
42. Yin, W.; Dadmun, M. A New Model for the Morphology of P3HT/PCBM Organic Photovoltaics From Small-Angle Neutron Scattering: Rivers and Streams. *ACS Nano* **2011**, *5*, 4756–4768.
43. Kumar, A.; Li, G.; Hong, Z.; Yang, Y. High Efficiency Polymer Solar Cells with Vertically Modulated Nanoscale Morphology. *Nanotechnology* **2009**, *20*, 165202.
44. Fang, L.; Wei, M.; Barry, C.; Mead, J. Effect of Spin Speed and Solution Concentration on the Directed Assembly of Polymer Blends. *Macromolecules* **2010**, *43*, 9747–9753.
45. Kargupta, K.; Sharma, A. Templating of Thin Films Induced by Dewetting on Patterned Surfaces. *Phys. Rev. Lett.* **2001**, *86*, 4536–4539.
46. Wang, X.; Ederth, T.; Inganäs, O. In Situ Wilhelmy Balance Surface Energy Determination of Poly(3-Hexylthiophene) and Poly(3,4-Ethylenedioxythiophene) during Electrochemical Doping–Dedoping. *Langmuir* **2006**, *22*, 9287–9294.
47. Dann, J. Forces Involved in the Adhesive Process:: I. Critical Surface Tensions of Polymeric Solids as Determined with Polar Liquids. *J. Colloid Interface Sci.* **1970**, *32*, 302–320.
48. Karim, A.; Douglas, J.; Lee, B.; Glotzer, S.; Rogers, J.; Jackman, R.; Amis, E.; Whitesides, G. Phase Separation of Ultrathin Polymer-Blend Films on Patterned Substrates. *Phys. Rev. E* **1998**, *57*, 6273–6276.
49. Wunderlich, B. Reversible Crystallization and the Rigid–Amorphous Phase in Semicrystalline Macromolecules. *Prog. Polym. Sci.* **2003**, *28*, 383–450.
50. Yang, L.; Zhou, H.; You, W. Quantitatively Analyzing the Influence of Side Chains on Photovoltaic Properties of Polymer–Fullerene Solar Cells. *J. Phys. Chem. C* **2010**, *114*, 16793–16800.
51. Price, S. C.; Stuart, A. C.; Yang, L.; Zhou, H.; You, W. Fluorine Substituted Conjugated Polymer of Medium Band Gap Yields 7% Efficiency in Polymer–Fullerene Solar Cells. *J. Am. Chem. Soc.* **2011**, *133*, 4625–4631.
52. Chabinyc, M. L. X-Ray Scattering from Films of Semiconducting Polymers. *Polym. Rev.* **2008**, *48*, 463–492.
53. Yamamoto, T.; Arai, M.; Kokubo, H.; Sasaki, S. Copolymers of Thiophene and Thiazole. Regioregulation in Synthesis, Stacking Structure, and Optical Properties. *Macromolecules* **2003**, *36*, 7986–7993.
54. Kline, R. J.; Delongchamp, D. M.; Fischer, D. A.; Lin, E. K.; Richter, L. J.; Chabinyc, M. L.; Toney, M. F.; Heeney, M.; McCulloch, I. Critical Role of Side-Chain Attachment Density on the Order and Device Performance of Polythiophenes. *Macromolecules* **2007**, *40*, 7960–7965.
55. Cho, E.; Risko, C.; Kim, D.; Gysel, R.; Cates Miller, N.; Breiby, D. W.; McGehee, M. D.; Toney, M. F.; Kline, R. J.; Bredas, J.-L. Three-Dimensional Packing Structure and Electronic Properties of Biaxially Oriented Poly(2,5-bis(3-alkylthiophene-2-yl)thieno[3,2-b]thiophene) Films. *J. Am. Chem. Soc.* **2012**, *134*, 6177–6190.
56. Lu, X.; Hlaing, H.; Germack, D. S.; Peet, J.; Jo, W. H.; Andrienko, D.; Kremer, K.; Ocko, B. M. Bilayer Order in a Polycarbazole-Conjugated Polymer. *Nat. Commun.* **2012**, *3*, 795.
57. Mayer, A. C.; Toney, M. F.; Scully, S. R.; Rivnay, J.; Brabec, C. J.; Scharber, M.; Koppe, M.; Heeney, M.; McCulloch, I.; McGehee, M. D. Bimolecular Crystals of Fullerenes in Conjugated Polymers and the Implications of Molecular Mixing for Solar Cells. *Adv. Funct. Mater.* **2009**, *19*, 1173–1179.
58. Seitz, O.; Böcking, T.; Salomon, A.; Gooding, J. J.; Cahen, D. Importance of Monolayer Quality for Interpreting Current Transport Through Organic Molecules: Alkyls on Oxide-Free Si. *Langmuir* **2006**, *22*, 6915–6922.